physica status solidi b
www.pss-b.com



# Investigation of Gamma-Radiation Shielding Properties of Cadmium Bismuth Borate Glass Experimentally and by Using XCOM Program and MCNP5 Code

*Yasser Saleh Mustafa Alajerami, David Drabold, M. H. A. Mhareb, Katherine Leslee A. Cimatu, Gang Chen, and K. M. Abushab*

**New glass systems of bismuth borate with various concentrations of cadmium oxide are prepared based on the melt-quenching method. The X-ray diffraction (XRD) reveals a fully amorphous structure of the prepared glasses (S1–S4), and the UV–vis results display good transparency (>50%) in the visible and near-UV region. In addition, the radiation shielding properties (mass attenuation coefficient, half-value layer, tenth value layer, mean free path, effective atomic number, and electron density) of the new glass system are determined at selected energies experimentally and by using MCNP5 simulation code and XCOM computer program. Based on the calculated relative difference, the obtained values from MCNP5 and XCOM are in good agreement with the experimental data. The mean free path of the current systems (particularly S4) shows optimistic results when compared with the barite and chalcocite concretes.**

## 1. Introduction

Recently, borate glasses with different oxide modifiers have received extensive interest from researchers. This type of glass exhibits desirable properties such as low cost, simple preparation, high transparency, chemical durability, and high thermal stability. These features recommend borate glass for solid-state lasers, radiation dosimeters, telecommunication devices, and radiation shielding materials.[1–4] Although ionizing radiation has essential applications in medical and industrial fields, this radiation has an adverse effect on human biological tissue. Great efforts and financial investments have been made to protect patients, employees, and the public from radiation.

For several years, concrete and lead shielding materials have been used for medical facilities and nuclear plants. Many disadvantages have been reported with concrete such as bacterial corrosion, leaching, expansion and aggregation, unrecyclable, and opaque to visible light.[5–7] Metallic lead has been used most often as a radiation shielding material mainly because it provides an effective shielding against penetrative radiation. In addition, it has a high atomic number, high density, low cost, and easy processability. However, metallic lead (Pb) is known for its toxicity, leads to environmental pollution, and has an extremely low level of neutron absorption.[8–11] Most of these drawbacks can be exceeded by glassy materials, which are effective attenuators, recyclable, hard, brittle, and transparent to visible light.[3,12] The bismuth borate glasses have received attention from researchers due to its clear potential applications. In addition to the previously mentioned glass features, this type of glass has low thermal expansion and shows high resistance to thermal shock.[1,12,13] Previous studies showed that excellent features were achieved by adding cadmium oxide (CdO) to the borate glass system (improved mechanical strength and density and maintained the amorphous structure of the glass network).[14–16] Both bismuth oxide and CdO provide compatibility with the borate glass system by increasing stabilization, improving chemical durability, and of course, increasing glass density.[17–20]

This study continues our previous research in determining the gamma shielding properties of new glassy borate systems with a constant amount of bismuth oxide and different CdO concentrations.[21] The gamma-ray shielding parameters of these samples were determined and compared with the standard radiation shielding (concrete and lead glass). The essential radiation shielding parameters such as mass attenuation coefficient

Dr. Y. S. M. Alajerami, Dr. D. Drabold, Dr. G. Chen
Department of Physics and Astronomy
Ohio University
Athens, OH 45701, USA

Dr. Y. S. M. Alajerami, Dr. K. M. Abushab
Medical Imaging Department
Applied Medical Sciences Faculty
Al Azhar University-Gaza
Jamal Abdl Naser St., Gaza Strip, P.O. BOX 1277, Gaza, Palestine

Dr. M. H. A. Mhareb
Department of Physics
College of Science
Imam Abdulrahman Bin Faisal University
P.O. Box 1982, Dammam 31441, Saudi Arabia

Dr. M. H. A. Mhareb
Basic and Applied Scientific Research Center
Imam Abdulrahman Bin Faisal University
P.O. Box 1982, Dammam 31441, Saudi Arabia

Dr. K. L. A. Cimatu
Department of Chemistry and Biochemistry
Ohio University
Athens, OH 45701, USA

The ORCID identification number(s) for the author(s) of this article can be found under https://doi.org/10.1002/pssb.202000417.

**DOI: 10.1002/pssb.202000417**

 

($\mu/\rho$), half-value layer (HVL), tenth value layer (TVL), mean free path (MFP), effective atomic number ($Z_{eff}$), and electron density ($N_e$) were estimated and calculated by using the Monte-Carlo N-particle transport code MCNP5 and the XCOM computer program. In addition, to verify the simulated and calculated results, the obtained values were compared with experimental values by establishing a compatible irradiation setup to determine the shielding parameters.

## 2. Experimental Section

### 2.1. Glass Preparation

Four borate glass systems were prepared based on the conventional quenching method according to the following formula

$$(70 - x)\%B_2O_3 - 30\%Bi_2O_3 - x\mathrm{CdO} \quad (x\colon 0,\ 5,\ 10,\ \text{and } 15\ \text{mol\%}) \tag{1}$$

As usual, the required quantities of the proposed chemicals were taken as powders and mixed well mechanically, and then melted in alumina crucibles at 1100 °C for 60–70 min (depend on CdO concentration). The melt was mixed during the melting process and finally poured into preheated pouring plates (300 °C) with rectangular molds. Prepared samples were kept 3 h to remove internal stress then cooled down slowly ($-10\,°\mathrm{C\,min^{-1}}$) to the room temperature.

### 2.2. Density and Molar Volume Measurements

The densities of the prepared samples were determined based on Archimedes principle (Equation (1)) by using toluene as the immersion fluid ($0.865\ \mathrm{g\,cm^{-3}}$). All densities were measured at room temperature and the measurement was repeated 3 times for each sample. Based on the obtained densities and molecular weight of the proposed composition ($M$), the molar volume ($V_m$) was calculated for all prepared samples (Equation (3)).

$$\rho = \frac{0.865\, W_{air}}{(W_{air} - W_{liquid})} \tag{2}$$

$$V_m = \frac{M}{\rho} \tag{3}$$

Here, the $W_{air}$ represents the sample's weight in the air and $W_{liquid}$ denotes the sample's weight in liquid.

### 2.3. UV–vis Spectroscopy and Bandgap

Shimadzu 3101 absorption spectrophotometer was utilized to obtain the absorption and transmittance spectra for current glass samples from 300 to 900 nm at room temperature. The bandgap ($E_g$) was determined from the UV absorption edge by utilizing Mott and Davis relation as illustrated below[22]

$$h\nu\alpha = A(h\nu - Eg)^n \tag{4}$$

where $\alpha$, $A$, and $h\nu$ denote the absorption coefficient, constant, and photon energy, respectively.

### 2.4. Irradiation Setup

In the current study, the glasses were irradiated with different energy levels of gamma rays obtained from radiation sources located in the Edwards Nuclear Accelerator Laboratory at Ohio

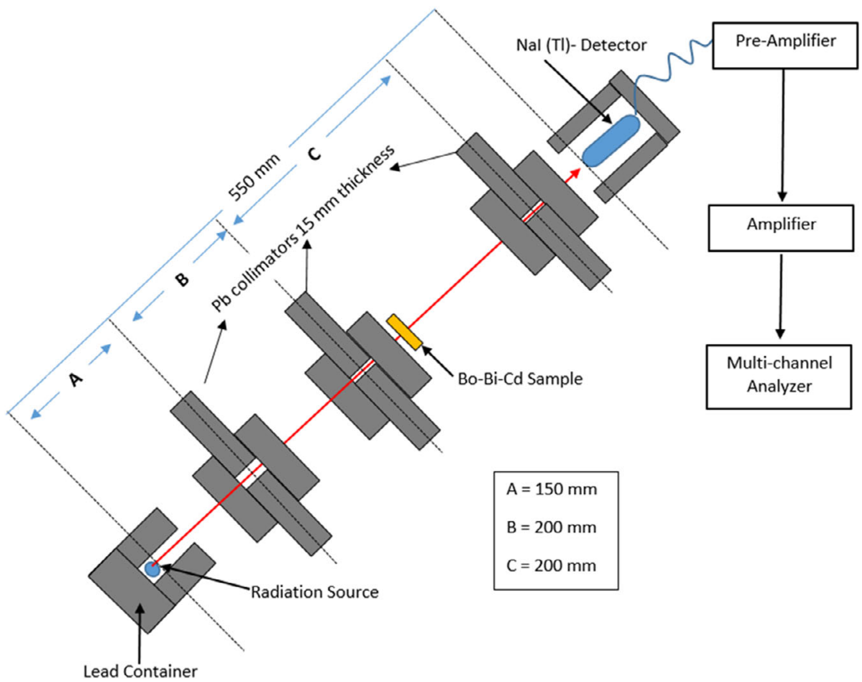


**Figure 1.** Schematic view for the setup of the irradiation process.

University, USA. The experimental setup of the irradiation and detection process is shown in **Figure 1**. Five different gamma-ray sources $^{57}$Co (122 keV), $^{133}$Ba (356 keV), $^{137}$Cs (662 keV), $^{60}$Co (1173 and 1332 keV), and $^{22}$Na (511 and 1275 keV) were used to irradiate the prepared glasses. These 12 samples (3 for each concentration) with a thickness range of 0.211–0.315 cm were prepared for irradiation and placed after the second lead collimator, as shown in Figure 1. A 3″ × 3″ NaI(Tl) scintillation detector connected with a preamplifier and an amplifier was used as the radiation detector to collect transmitted gamma ray from irradiated samples and convert the analog signal to electron counts. A gamma-ray spectrometer with a 16 K multichannel analyzer (CANBERRA Industries) and an energy resolution of 7.5% at 661.6 keV for a gamma ray from Cs-137 were used to collect incident and transmitted intensities $I_0$ and $I$, respectively. The distance between the radiation source and NaI detector was 65 cm for all irradiation process (either with or without samples).

Three Pb collimator sets with whole different sizes were used to avoid the detection of background radiation. Both radiation source and detector were housed in a lead shield (C-shape). Finally, the spectrometer was frequently calibrated for each trial and any given energy.

All radiation shielding equations needed for evaluation and measurement of shielding properties are shown in **Table 1**.

**Table 1.** Mathematical expressions for evaluating the radiation shielding properties.

| Parameter | Formula | Symbols |
|---|---|---|
| Linear attenuation coefficient ($\mu$)[38] | $\mu = \ln\left(\frac{I_0}{I}\right)\left(\frac{1}{t}\right)$ | $I_0$: intensity without sample |
| | | $I$: intensity with sample |
| | | $t$: the thickness of the sample |
| Total photon interaction cross section ($\sigma_t$)[39] | $\sigma_t = \frac{M\mu_m}{N_A}$ | $N_A$: Avogadro's number |
| | | $M$: the molecular weight of glass |
| Mean free path (MFP)[40] | $\mathrm{MFP} = 1/\mu$ | $\mu$: linear attenuation coefficient |
| Tenth value layer (TVL)[40] | $\mathrm{TVL} = (\ln 10)/\mu$ | |
| Half value layer (HVL)[40] | $\mathrm{HVL} = \frac{0.693}{\mu}$ | |
| Effective atomic number ($Z_{eff}$)[41] | $Z_{eff} = \frac{\sum_i f_i A_i \left(\frac{\mu}{\rho}\right)_i}{\sum_j f_j \frac{A_j}{Z_j} \left(\frac{\mu}{\rho}\right)_j}$ | $f_i$ is the fractional abundance of the element $i$, $A_i$ is the atomic weight, and $Z_i$ is the atomic number. |
| Effective electron number ($N_e$)[42] | $N_e = \left(\frac{Z_{eff}}{M}\right) N_A \sum_i n_i$ | $M$: molecular weight |
| | | $n_i$: number of formula units |

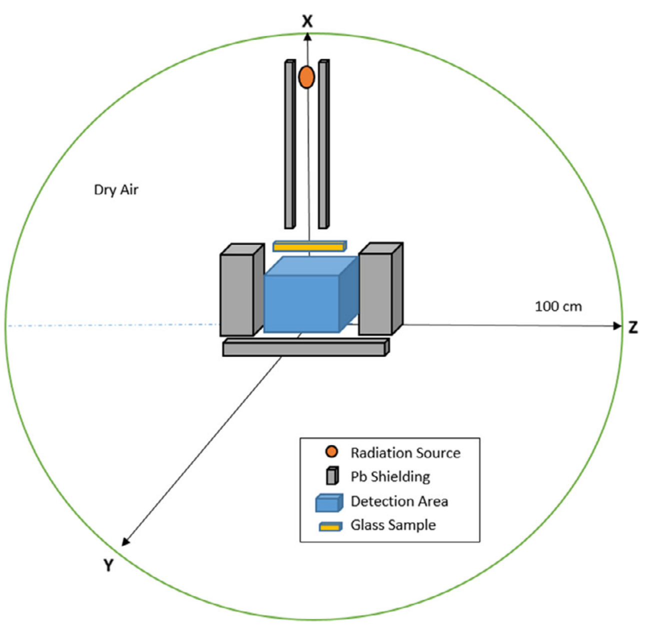


**Figure 2.** Total simulation geometry using MCNP5.

## 2.5. XCOM Program

The theoretical mass attenuation coefficients ($\mu/\rho$) for the prepared glasses were obtained from the known computer program XCOM.[23] This program can estimate the mass attenuation coefficient of an element, compound, and mixture at different energy

**Table 2.** Chemical composition, density, and molar volume of the prepared samples.

| Sample code | Chemical composition [mol%] | | | Density [g cm$^{-3}$] | Molar volume [cm$^3$ mol$^{-1}$] | Bandgap ($E_g$) [eV] |
|---|---|---|---|---|---|---|
| | $Bi_2O_3$ | CdO | $B_2O_3$ | | | |
| S1 | 30 | 0 | 70 | 4.315 | 46.689 | 2.907 |
| S2 | 30 | 5 | 65 | 4.711 | 40.641 | 3.106 |
| S3 | 30 | 10 | 60 | 5.068 | 38.358 | 3.259 |
| S4 | 30 | 15 | 55 | 5.375 | 36.714 | 3.442 |


**Figure 3.** The new prepared glasses (S1–S4).

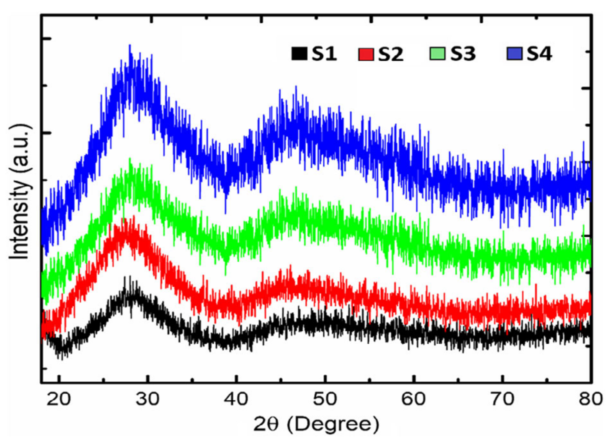


**Figure 4.** XRD of the new prepared glass systems.

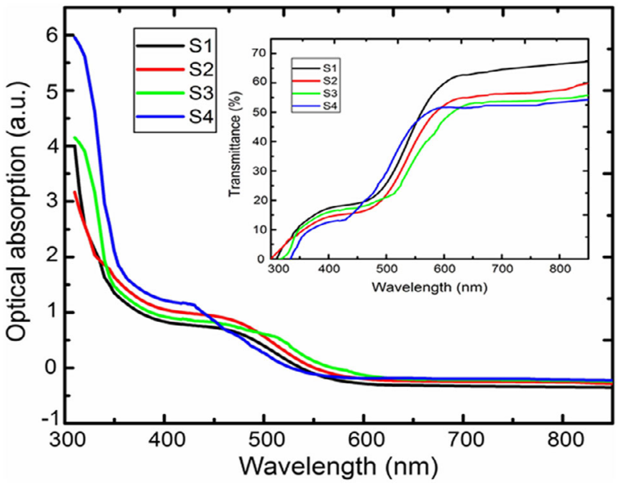


**Figure 5.** The optical absorption of all prepared glasses (inset, corresponding transmission spectra) in the wavelength range 300–800 nm.

levels (0.001 up to $10^5$ MeV). Based on the estimated $\mu/\rho$ and the calculated densities, the linear attenuation coefficient can be easily determined. The other radiation shielding parameters were also determined by using the equations from Table 1 (except the first equation).

### 2.6. MCNP5 Simulation Code

The current experimental setup was simulated by MCNP5, which is used for modeling the interaction of electromagnetic radiation (X-ray), photon (gamma ray), and particles (electron and neutron). Previous related studies have validated and reported the high efficiency of MCNP5 to evaluate and estimate radiation shielding parameters.[24–27]

In the current study, MCNP5 was used to estimate the newly prepared glasses' radiation shielding parameters. The simulation was applied in a sphere of 100 cm radius filled with dry air ($\rho = 1.205 \times 10^{-3}$ g cm$^{-3}$), as shown in **Figure 2**. The radiation source was assumed as a point source with a monoenergetic beam emission and positioned perpendicularly to the front surface of the glass sample (in the $x$-axis direction). The irradiation process was completely guided by Pb shielding collimators to eliminate the possibility of background radiation detection. The simulation was repeated based on the mol% of CdO and

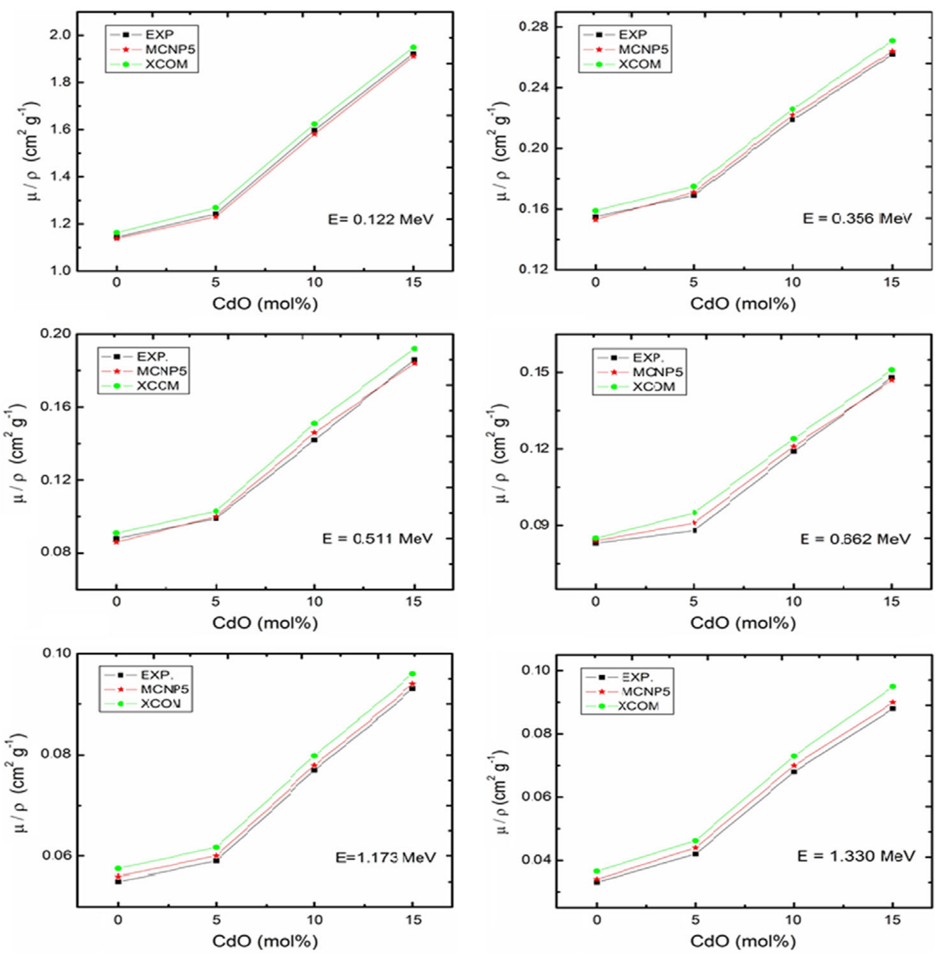


**Figure 6.** Dependency of $\mu/\rho$ of the $Bi_2O_3$–$x$–$B_2O_3$ glasses on $x$-CdO contents at different energy levels (comparison is made between experimental, MCNP5, and XCOM values).

**Table 3.** Mass attenuation coefficients at specific energies (experimental, MCNP, and XCOM) (Exp., Experiment).

| Energy [MeV] | | S1 | S2 | S3 | S4 |
|---|---|---|---|---|---|
| 0.122 | Exp. | $1.144 \pm 0.003$ | $1.242 \pm 0.005$ | $1.598 \pm 0.006$ | $1.932 \pm 0.003$ |
| | MCNP5 | $1.139 \pm 0.004$ | $1.231 \pm 0.003$ | $1.581 \pm 0.005$ | $1.921 \pm 0.005$ |
| | XCOM | 1.153 | 1.269 | 1.624 | 1.949 |
| 0.356 | Exp. | $0.149 \pm 0.003$ | $0.169 \pm 0.005$ | $0.219 \pm 0.004$ | $0.259 \pm 0.006$ |
| | MCNP5 | $0.157 \pm 0.004$ | $0.172 \pm 0.002$ | $0.221 \pm 0.003$ | $0.268 \pm 0.003$ |
| | XCOM | 0.160 | 0.177 | 0.226 | 0.271 |
| 0.511 | Exp. | $0.094 \pm 0.002$ | $0.101 \pm 0.003$ | $0.142 \pm 0.003$ | $0.186 \pm 0.003$ |
| | MCNP5 | $0.097 \pm 0.003$ | $0.103 \pm 0.004$ | $0.146 \pm 0.005$ | $0.184 \pm 0.004$ |
| | XCOM | 0.101 | 0.108 | 0.151 | 0.188 |
| 0.662 | Exp. | $0.083 \pm 0.003$ | $0.009 \pm 0.003$ | $0.119 \pm 0.004$ | $0.143 \pm 0.004$ |
| | MCNP5 | $0.086 \pm 0.003$ | $0.091 \pm 0.004$ | $0.121 \pm 0.003$ | $0.146 \pm 0.003$ |
| | XCOM | 0.091 | 0.097 | 0.128 | 0.152 |
| 1.173 | Exp. | $0.056 \pm 0.003$ | $0.065 \pm 0.003$ | $0.078 \pm 0.003$ | $0.094 \pm 0.003$ |
| | MCNP5 | $0.057 \pm 0.004$ | $0.068 \pm 0.004$ | $0.080 \pm 0.004$ | $0.096 \pm 0.005$ |
| | XCOM | 0.060 | 0.070 | 0.084 | 0.101 |
| 1.332 | Exp. | $0.044 \pm 0.003$ | $0.052 \pm 0.003$ | $0.067 \pm 0.004$ | $0.085 \pm 0.004$ |
| | MCNP5 | $0.045 \pm 0.004$ | $0.054 \pm 0.004$ | $0.071 \pm 0.003$ | $0.087 \pm 0.008$ |
| | XCOM | 0.047 | 0.057 | 0.081 | 0.091 |

repeated 3 times for each sample (S1–S4). All required data cards and commands such as energy (ERG), type of particle (PAR), position (POS), and beam direction (DIR) were defined accordingly. Several termination steps were applied to reduce errors and variance, such as increasing the number of histories (NPS $> 10^8$), simplifying the geometry, and utilizing the CUTOFF option to eliminate low radiation ($<1$ keV). Regarding energy detection, mesh tally (type F4) was used to get the sum of all contributions in the proposed detecting area. All measurements (collimation thickness, distance from the source to detectors, and sample size) were set based on the experimental data.

## 3. Results and Discussion

Details about the prepared samples including sample code, mol% of chemical composition, measured densities, and molar volumes are shown in **Table 2**.

The density of the prepared samples increased gradually with the variation of CdO content from 0 to 15 mol%. The calculated densities were in the range of 4.315–5.375 g cm$^{-3}$ with a probable error of 0.005. The density is composition-dependent and the observed increase in the value can be attributed to the high molecular weight of CdO (128.41 g mol$^{-1}$) compared with that of $B_2O_3$ (32.01 g mol$^{-1}$). Reverse relation was reported with the molar volume; from Table 2, the values were reduced from 46.689 cm$^3$ mol$^{-1}$ for S1 to 36.714 cm$^3$ mol$^{-1}$ for S4.

The prepared glass was highly transparent, and gradually changed into brown with the increase in $Bi_2O_3$, as shown in **Figure 3**.

The structure of the current samples was examined with X-ray diffraction (XRD). The amorphous state was confirmed by the continuous diffraction pattern with no sharp peak and the broad peak centered on $2\theta = 25°$ (**Figure 4**). The peak broadening can be attributed to its amorphous structure.

**Figure 5** shows the optical absorption spectra for all prepared glasses in the range of 300–900 nm. The inset figure shows the calculated transmittance spectra obtained from the absorption values. All glass systems exhibit good transparencies (>50%) in the visible and near-UV region. This result is expected with a borate glass system. In all samples, the fraction of $B_2O_3$ is more than 50%, a fixed amount of $Bi_2O_3$ (30 mol%) and the amount of CdO does not exceed 15 mol%.

From Figure 5 and by using Mott and Davis equation, we can determine $E_g$. The $E_g$ was computed from the intercept horizontal axis of $h\nu$ and $(\alpha h\nu)^2$. This intercept can be drawn as a tangent line along the absorption edge $(\alpha h\nu)^2$ to reach the $h\nu$ ($x$-axis), this is called $E_g$. It can be noted from Table 2 that the bandgap results increase gradually with the addition of the CdO to the glass system that ascribed to the formation of bridging oxygen in the glass structure.[28,29]

### 3.1. Mass Attenuation Coefficient

The simulated (by MCNP5) and estimated (by XCOM) values of $\mu/\rho$ of the different glass systems are shown in **Figure 6** for different photon energy. The experimental data of $\mu/\rho$ of the same samples were compared with those obtained by MCNP5 and XCOM at specific energy levels (0.122, 0.356, 0. 511, 0.662, 1.173, and 1.330 MeV), as listed in **Table 3**. The values of $\mu/\rho$ that have been obtained experimentally and by simulation are the average of three repeating trials plus/minus the standard deviation of these trials, respectively.

The dependency of $\mu/\rho$ of the new glass samples on the concentration of CdO at different energy levels, by using irradiation

**Table 4.** Relative difference between the MCNP5/XCOM results and the experimental values.

| Glass code | Incident photon energy [MeV] | | | | | | | | | | | |
|---|---|---|---|---|---|---|---|---|---|---|---|---|
| | 0.122 | | 0.365 | | 0.511 | | 0.662 | | 1.173 | | 1.332 | |
| | MCNP | XCOM | MCNP | XCOM | MCNP | XCOM | MCNP | XCOM | MCNP | XCOM | MCNP | XCOM |
| S1 | 0.437 | 0.787 | 5.370 | 7.382 | 3.191 | 7.447 | 2.381 | 7.143 | 1.786 | 7.142 | 2.273 | 6.818 |
| S2 | 0.886 | 2.174 | 1.775 | 4.734 | 1.980 | 6.930 | 1.111 | 7.778 | 4.615 | 7.692 | 3.846 | 7.694 |
| S3 | 1.064 | 1.627 | 0.913 | 3.196 | 2.817 | 6.338 | 1.681 | 7.563 | 2.564 | 7.692 | 0 | 6.944 |
| S4 | 0.570 | 0.880 | 3.474 | 4.633 | 1.075 | 1.075 | 2.098 | 6.294 | 2.128 | 7.447 | 2.353 | 7.059 |

setup, simulation, and XCOM program, is displayed in Figure 6. Good agreement was reported between the three estimation methods at a photon energy of 0.122, 0.356, 0.511, 0.662, 1.173, and 1.332 MeV (with insignificant variations). Also, the mass attenuation coefficient was increased by increasing CdO content (mol%) and decreased by increasing the energy level. This behavior indicates that the higher interactions of a photon with a glass system take place at high CdO and low photon energy. Based on the values obtained from Table 3 and Figure 6, as the energy changed from 0.122 to 0.511 MeV, the $\mu/\rho$ decreased quickly (photoelectric effect abundancy $Z^{4.0-4.5}/E^3$), and no substantial variation at the energy range of 0.511 and 1.332 MeV due to the high possibility of Compton scattering $(Z/E)$.[26,30]

**Table 5.** HVL of the new glasses at specific energies (experimental, MCNP, and XCOM) (Exp., Experiment).

| Energy [MeV] | | S1 | S2 | S3 | S4 |
|---|---|---|---|---|---|
| 0.122 | Exp. | 0.172 | 0.150 | 0.109 | 0.166 |
| | MCNP5 | 0.173 | 0.152 | 0.110 | 0.151 |
| | XCOM | 0.171 | 0.147 | 0.107 | 0.083 |
| 0.356 | Exp. | 1.323 | 1.105 | 0.797 | 0.706 |
| | MCNP5 | 1.256 | 1.086 | 0.790 | 0.675 |
| | XCOM | 1.232 | 1.055 | 0.773 | 0.598 |
| 0.511 | Exp. | 2.240 | 1.89 | 1.23 | 0.991 |
| | MCNP5 | 2.032 | 1.867 | 1.196 | 0.941 |
| | XCOM | 1.842 | 1.667 | 1.156 | 0.862 |
| 0.662 | Exp. | 2.375 | 2.122 | 1.505 | 1.117 |
| | MCNP5 | 2.292 | 2.052 | 1.443 | 1.119 |
| | XCOM | 2.142 | 1.849 | 1.353 | 1.046 |
| 1.173 | Exp. | 3.651 | 3.012 | 2.328 | 1.781 |
| | MCNP5 | 3.459 | 2.746 | 2.183 | 1.719 |
| | XCOM | 3.286 | 2.434 | 2.055 | 1.605 |
| 1.332 | Exp. | 3.805 | 3.199 | 2.361 | 2.001 |
| | MCNP5 | 3.741 | 3.131 | 2.279 | 1.933 |
| | XCOM | 3.651 | 3.012 | 2.156 | 1.781 |

The relative difference (RD) between the three estimation methods (experimental, MCNP5, and XCOM) of the calculated values was calculated according to the following equation[27]

$$\text{RD} = \frac{\text{Theoretical} - \text{Experimental}}{\text{Experimental}} \times 100 \tag{5}$$

**Table 4** shows the RD values for MCNP and XCOM results for all samples. The RD values show close agreement between mass attenuation coefficients obtained by experiment, MCNP5, and XCOM. This agreement between experiment and MCNP5 was quite encouraging, the RD was in the range of 0–5.37%, and for XCOM values were in the range of 0.787–7.778%. This RD is acceptable and supports the usage of MCNP5 to estimate glass shielding properties for other glass compositions.

**Table 5** shows the HVL of the new glasses at different concentrations of CdO and specific energy levels. The glass with the smallest HVL means the highest efficiency to attenuate the photon beam. The smaller HVL indicates that this composition is cost-effective, high transparent, and requires simple fabrication.[30] **Figure 7**a shows the dependency of HVL on the CdO concentration; gradual reduction in the HVL values is reported with increasing CdO concentration. We can also say that MCNP5 showed closer agreement with the experimental data compared with XCOM values. Figure 7b shows the glasses' HVL of S4 (the smallest HVL) at different energy levels using the three estimation methods (experimental, MCNP5, and XCOM). The HVL increased gradually with increasing energy of the incident photon (0.122–1.330 MeV). As discussed in the mass attenuation coefficients, the HVL values' variation with increasing energy of an incident photon is attributed to the variations of dominance photon interaction.[30–33]

The TVL of the prepared glasses was also calculated. The TVL can be defined as the attenuator thickness that can reduce the photon intensity to 10th of its initial intensity. **Figure 8** shows a simple comparison of the TVL (experimental values) of all prepared glasses as a function of photon energies. The TVL values have increased with increasing the incident photon (0.112–1.332 MeV) and decreased with increased CdO content, which is attributed to increasing sample density.[32]

The average distance between two successive interactions of a photon (or moving particle) inside a target material is known

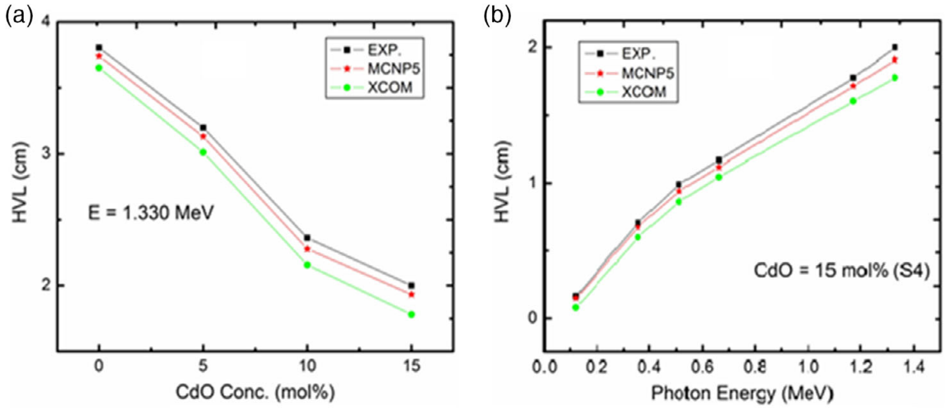


**Figure 7.** a) The HVL of the prepared glasses with *x*-concentrations of CdO at different energy levels. b) The HVL of S4 (the smallest HVL) at different energy levels using the three estimation methods (experimental, MCNP5, and XCOM).

 

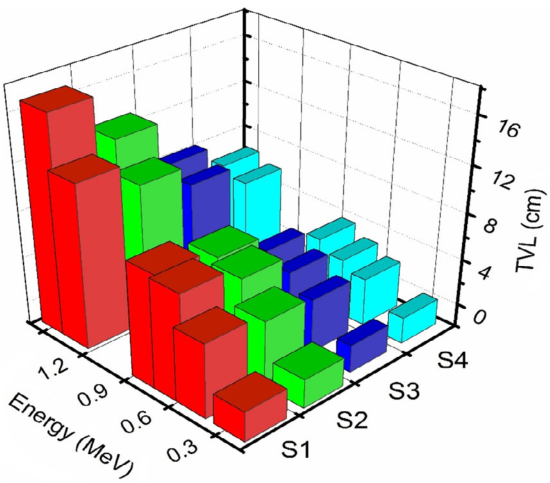


**Figure 8.** Comparison between TVL of different glass systems as a function of photon energies.

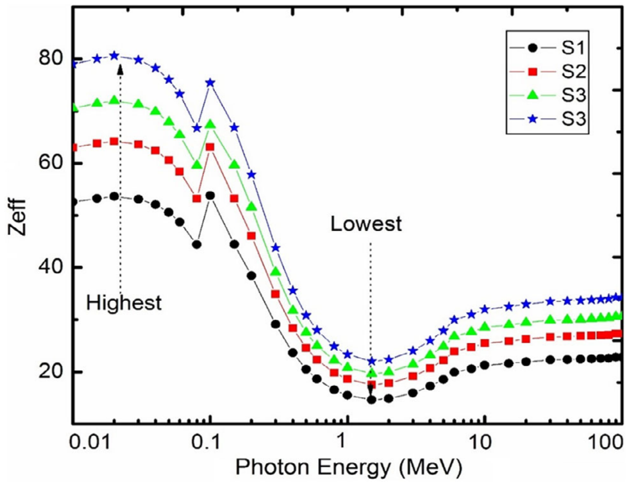


**Figure 9.** Variation of $Z_{eff}$ of the prepared glasses with energy for the various concentrations of CdO.

as the MFP.[34] This concept indicates the photon direction, energy, and other particle properties significant for shielding consideration. The MFP of the current samples was calculated by using the equation listed in Table 1 and **Table 6**. The values were calculated by conducting the three estimation methods (experimental, MCNP5, and XCOM) and compared with the MFP of barite and chalcocite concretes. The lowest MFP is reported in the S4 glass sample (the highest CdO content) and it is 2 times lower than the values obtained with barite and chalcocite concretes.

The $Z_{eff}$ of all samples was obtained using the XCOM program for a high range of energy, starting from 0.01 up to 100 MeV, as shown in **Figure 9**. Generally, the values of $Z_{eff}$ decreased by increasing photon energy and increased by increasing CdO content. The highest $Z_{eff}$ was reported at 0.02 MeV (53.611) and the lowest values at 0.15 MeV (14.670). The abrupt features observed at 0.08 MeV, which is attributed to the K-edge of Bi.[35] The slight increase reported after the 3 MeV region attributed to the dominance of pair production in the energy level.[36]

Based on Table 1, the $Z_{eff}$ and effective electron density ($N_{eff}$) of the prepared glasses are calculated via experiment, MCNP5, and XCOM program and listed in **Table 7** and **8**, respectively. Regarding the values listed in Table 7, the comparison was performed based on the available six radiation sources used for experiment calculations (0.122–1.332 MeV). The $Z_{eff}$ at this energy range was increased with increasing photon energy

**Table 6.** Mean free path of the new prepared samples.

| Shielding material | Density [g cm$^{-3}$] | 0.122 MeV | | | 0.356 MeV | | | 0.511 MeV | | |
|---|---|---|---|---|---|---|---|---|---|---|
| | | Exp. | MCNP | XCOM | Exp. | MCNP | XCOM | Exp. | MCNP | XCOM |
| S1 | 4.315 | 0.249 | 0.250 | 0.247 | 1.909 | 1.812 | 1.179 | 3.233 | 2.933 | 2.659 |
| S2 | 4.711 | 0.217 | 2.199 | 0.212 | 1.594 | 1.567 | 1.522 | 2.722 | 2.695 | 2.406 |
| S3 | 5.068 | 0.158 | 0.161 | 0.155 | 1.151 | 1.140 | 1.115 | 1.775 | 1.726 | 1.669 |
| S4 | 5.375 | 0.121 | 0.122 | 0.120 | 0.903 | 0.873 | 0.863 | 1.258 | 1.271 | 1.244 |
| Barite concrete | 3.350 | – | 0.592 | 0.686 | – | 2.617 | 2.469 | – | 3.356 | 3.597 |
| Chalcocite concrete | 3.703 | – | 1.271 | 1.273 | – | 2.633 | 2.645 | – | 3.174 | 3.175 |
| Shielding material | Density [g cm$^{-3}$] | 0.662 MeV | | | 1.173 MeV | | | 1.332 MeV | | |
| | | Exp. | MCNP | XCOM | Exp. | MCNP | XCOM | Exp. | MCNP | XCOM |
| S1 | 4.315 | 3.428 | 3.308 | 3.092 | 5.268 | 4.991 | 4.741 | 7.295 | 6.322 | 5.268 |
| S2 | 4.711 | 3.061 | 2.961 | 2.668 | 4.346 | 3.963 | 3.513 | 5.614 | 4.990 | 4.346 |
| S3 | 5.068 | 2.172 | 2.083 | 1.954 | 3.360 | 3.150 | 2.964 | 3.761 | 3.545 | 3.111 |
| S4 | 5.375 | 1.659 | 1.602 | 1.509 | 2.570 | 2.437 | 2.316 | 2.888 | 2.689 | 2.570 |
| Barite concrete[a)] | 3.350 | 3.371 | 3.355 | 3.382 | – | 5.381 | 5.350 | 5.521 | 5.782 | 5.711 |
| Chalcocite concrete | 3.703 | – | 3.445 | 3.559 | – | 4.667 | 4.739 | – | 5.777 | 5.025 |

[a)]The MFP values of barite concrete and chalcocite concrete were obtained from previous studies.[26,43,44]

**Table 7.** Experimental, MCNP5, and XCOM values of $Z_{eff}$ of the new glasses.

| Shielding material | 0.122 MeV | | | 0.356 MeV | | | 0.511 MeV | | |
|---|---|---|---|---|---|---|---|---|---|
| | Exp. | MCNP | XCOM | Exp. | MCNP | XCOM | Exp. | MCNP | XCOM |
| S1 | 15.099 | 16.224 | 17.111 | 16.643 | 17.009 | 17.778 | 18.569 | 19.005 | 19.021 |
| S2 | 18.092 | 19.156 | 19.565 | 19.942 | 20.554 | 21.211 | 22.249 | 23.335 | 23.813 |
| S3 | 20.263 | 21.554 | 22.011 | 22.335 | 23.112 | 24.010 | 24.919 | 25.555 | 26.014 |
| S4 | 22.695 | 23.112 | 24.771 | 25.015 | 26.276 | 26.832 | 27.910 | 28.282 | 29.087 |
| Shielding material | 0.662 MeV | | | 1.173 MeV | | | 1.332 MeV | | |
| | Exp. | MCNP | XCOM | Exp. | MCNP | XCOM | Exp. | MCNP | XCOM |
| S1 | 19.718 | 20.221 | 21.005 | 21.179 | 22.022 | 22.898 | 21.456 | 22.221 | 23.833 |
| S2 | 23.626 | 24.777 | 25.112 | 25.377 | 26.266 | 27.066 | 25.709 | 26.410 | 28.332 |
| S3 | 26.461 | 27.890 | 28.044 | 28.423 | 29.029 | 29.789 | 28.795 | 29.033 | 30.774 |
| S4 | 29.637 | 30.111 | 31.088 | 31.833 | 31.935 | 32.994 | 32.250 | 33.012 | 33.876 |

**Table 8.** Experimental, MCNP5, and XCOM values of $N_e$ of the new glasses.

| Shielding material | 0.122 MeV | | | 0.356 MeV | | | 0.511 MeV | | |
|---|---|---|---|---|---|---|---|---|---|
| | Exp. | MCNP | XCOM | Exp. | MCNP | XCOM | Exp. | MCNP | XCOM |
| S1 | 9.125 | 9.138 | 9.149 | 5.711 | 5.705 | 5.720 | 3.986 | 3.993 | 4.011 |
| S2 | 9.255 | 9.267 | 9.288 | 5.426 | 5.433 | 5.452 | 4.111 | 4.108 | 4.116 |
| S3 | 9.424 | 9.430 | 9.442 | 5.548 | 5.552 | 5.565 | 4.769 | 4.777 | 4.785 |
| S4 | 9.118 | 9.927 | 9.934 | 5.582 | 5.487 | 5.499 | 4.878 | 4.883 | 4.892 |
| Shielding material | 0.662 MeV | | | 1.173 MeV | | | 1.332 MeV | | |
| | Exp. | MCNP | XCOM | Exp. | MCNP | XCOM | Exp. | MCNP | XCOM |
| S1 | 3.708 | 3.714 | 3.722 | 3.137 | 3.133 | 3.143 | 3.075 | 3.073 | 3.065 |
| S2 | 3.788 | 3.794 | 3.803 | 3.151 | 3.149 | 3.158 | 3.069 | 3.065 | 3.075 |
| S3 | 3.939 | 3.944 | 3.953 | 3.159 | 3.163 | 3.168 | 3.078 | 3.075 | 3.084 |
| S4 | 3.169 | 3.174 | 4.181 | 3.168 | 3.171 | 3.177 | 3.093 | 3.089 | 3.097 |

(dominant of pair production) and increased with increasing CdO content (S4 has the highest $\mu/\rho$ and density).

Regarding $N_e$ of the new glass systems, the $N_e$ relies on the $Z_{eff}$ of the material. Therefore, $N_e$ has increased by increasing the CdO concentration (replacement of boron element ($Z = 5$) by cadmium ($Z = 48$). The $N_e$ values vary with photon energy, attributed to the cross-section dependence, as discussed before.

The new glasses' performance in attenuation of gamma rays is determined in terms of radiation protection efficiency (RPE). This parameter was calculated from the values of $I$ and $I_0$ obtained from the experimental setup irradiation and based on the following equation[37]

$$\text{RPE} = \left(1 - \frac{I}{I_0}\right) \times 100 \tag{6}$$

**Figure 10** shows the calculation of RPEs for the new glasses for the selected six energies in the current study. The results show that the RPE values have decreased with the increasing energy of the incident photon. High performance was achieved at low energies (0.122, 0.356, and 0.511 MeV) and decreased with high energies (0.662, 1.173, and 1.332 MeV). The current values also show that the sample with a higher concentration of CdO (S4) has the highest attenuation efficiency than the other samples. This performance has wholly agreed with the results obtained in the effective atomic number. This reflects that replacing a lighter molecule ($B_2O_3$) with a heavier molecule (CdO) leads to an increase in the glasses' attenuation efficiencies.

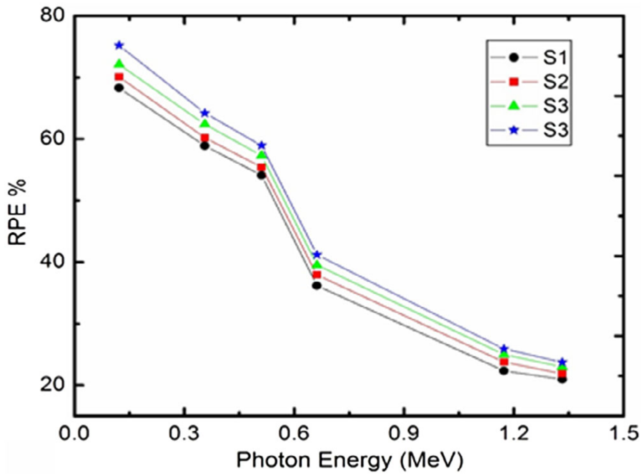


**Figure 10.** Experimental radiation protection efficiency of the prepared glasses at different photon energies.

## 4. Conclusion

Bismuth borate glass systems ($30Bi_2O_3 + 70–xB_2O_3$) with different concentrations of CdO ($x = 0–15$ mol%) were prepared by the conventional melt-quenching technique. This study aims to increase glass density (replacing lighter atoms with heavier atoms) while maintaining borate glass transparency. Structural characterization for the newly prepared glasses was conducted by utilizing XRD and UV–vis spectroscopy. Synchronize increase in the prepared glasses' density was reported with the gradual rise of CdO with a reduction of molar volume and energy bandgap. The radiation properties were determined experimentally at specific energies (0.112, 0.356, 0.511, 0.662, 1.173, and 1.332 MeV) and compared with MCNP5 and XCOM simulated values. The new glasses show optimistic radiation shielding properties (high mass attenuation coefficients, accepted atomic number, and shorter MFP and TVL values). Compared with barite and chalcocite concretes, the proposed composition is highly recommended for radiation shielding applications.

## Acknowledgements

The authors would like to gratefully acknowledge the financial support obtained from International Institute of Education (IIE)—Fulbright Program—and from Nanoscale Quantum Phenomena Institute (NQPI)/Ohio University. In addition, G.C. and D.A.D. acknowledge the support from US National Science Foundation under Grant DMR-1507670.

 

## Conflict of Interest

The authors declare no conflict of interest.

## Keywords

bismuth borate glass, MCNP5, radiation shielding, XCOM

Received: July 29, 2020
Revised: November 4, 2020
Published online:

[1] M. G. Dong, M. I. Sayyed, G. Lakshminaravana, M. Çelikbilek Ersundu, A. E. Ersundud, P. Nayar, M. A. Mahdi, *J. Non-Cryst. Solids* **2017**, *468*, 12.
[2] Y. S. M. Alajerami, S. Hashim, W. M. S. Hassan, A. T. Ramli, *Physica B* **2012**, *407*, 2390.
[3] S. Sunil Kumar, J. Khatei, S. Kasthurirengan, K. S. R. Koteswara Rao, K. P. Ramesh, *J. Non-Cryst. Solids* **2011**, *357*, 842.
[4] M. H. A. Mhareb, S. Hashim, S. K. Ghoshal, Y. S. M. Alajerami, M. A. Saleh, S. A. B. Azizan, M. A. Karim, *J. Radioanal. Nucl. Chem.* **2015**, *2*, 469.
[5] C. M. Lee, Y. H. Lee, K. J. Lee, *Prog. Nucl. Energy.* **2007**, *49*, 303.
[6] M. Kurudirek, Y. Ozdemir, O. Simsek, R. Durak, *J. Nucl. Mater.* **2010**, *407*, 110.
[7] R. Bagheri, A. K. Moghaddam, Hassan Yousefnia, *Nucl. Eng. Technol.* **2017**, *49*, 216.
[8] Agency for Toxic Substances and Disease Registry (ATSDR), *Toxicological Profile for Lead (Draft for Public Comment)*, U.S. Department of Health and Human Services, Public Health Service, Atlanta, GA **2019**.
[9] O. Oyar, A. Kislalioglu, *Diagn. Interv. Radiol.* **2012**, *18*, 147.
[10] V. P. Singh, N. M. Badiger, S. Kothan, S. Kaewjaeng, T. Korkut, H. J. Kim, J. Kaewkhao, *Nucl. Sci. Tech.* **2016**, *27*, 103.
[11] J. P. McCaffrey, H. Shen, B. Downton, E. Mainegra-Hing, *Med. Phys.* **2007**, *34*, 530.
[12] S. R. Manohara, S. M. Hanagodimath, L. Gerward, *J. Nucl. Mater.* **2009**, *393*, 465.
[13] P. Kaur, K. J. Singh, M. Kurudirek, S. Thakur, *Spectrochim. Acta A: Mol. Biomol. Spectrosc.* **2019**, *223*, 117309.
[14] V. Sharma, S. Singh, G. Mudahar, K. Thind, *New J. Glass Ceram.* **2012**, *2*, 128.
[15] S. Bahammam, S. Abd El Al, F. M. Ezz-Eldin, *Results Phys.* **2017**, *7*, 241.
[16] R. Ezhil Pavai, P. Shalini Priya Dharsini, *Sci. Res.* **2017**, *8*, 17242.
[17] K. Kirdsiri, J. Kaewkhao, N. Chanthima, P. Limsuwan, *Ann. Nucl. Energy*, **2011**, *38*, 1438.
[18] K. Singh, H. Singh, V. Sharma, R. Nathuram, A. Khanna, R. Kumar, S. S. Bhatti, H. S. Sahota, *Nucl. Instrum. Methods B* **2002**, *194*, 1.
[19] N. Singh, K. J. Singh, K. Singh, H. Singh, *Nucl. Instrum. Methods B* **2004**, *225*, 305.
[20] W. M. Abd-Allah, A. M. Fayad, H. A. Saudi, *Opt. Quantum Electron.* **2019**, *51*, 165.
[21] Y. S. Alajerami, D. Drabold, M. Mhareb, K. A. Leslee Cimatu, G. Chen, *Ceram. Int.* **2020**, *46*, 12718.
[22] N. F. Mott, E. A. Davis, *Materials*, Clarendon Press, Oxford, **1971**.
[23] M. J. Berger, J. H. Hubbell, *XCOM: Photon Cross Sections on a Personal Computer*, NBSIR 87-3597, National Bureau of Standards, Gaithersburg, MD **1987**.
[24] M. G. Dong, R. El-Mallawany, M. I. Sayyed, H. O. Tekin, *Radiat. Phys. Chem.* **2017**, *141*, 172.
[25] H. O. Tekin, U. Kara, *J. Commun. Comput.* **2016**, *13*, 32.
[26] K. A. Mahmoud, M. I. Sayyed, O. L. Tashlykov, *Radiat. Phys. Chem.* **2019**, *165*, 108426.
[27] M.Kh. Hamad, M. H. A. Mhareb, Y. S. Alajerami, M. I. Sayyed, G. Saleh, Y. Maswadeh, Kha. Ziq, *Radiat. Phys. Chem.* **2020**, *174*, 108920.
[28] M. H. A. Mhareb, M. Alqahtani, F. Alshahri, Y. S. M. Alajerami, N. Saleh, N. Alonizan, M. I. Sayyed, M. G. B. Ashiq, T. Ghrib, S. Ibrahim Al-Dhafar, T. Alayed, M. A. Morsy, *J. Non-Cryst. Solids* **2020**, *541*, 120090.
[29] M. H. A. Mhareb, Y. S. M. Alajerami, M. I. Sayyed, N. Dwaikat, M. Alqahtani, F. Alshahri, N. Saleh, N. Alonizan, T. Ghrib, S. Ibrahim Al-Dhafar, *J. Non-Cryst. Solids* **2020**, *550*, 120360.
[30] T. Kaur, J. Sharma, T. Singh, *Prog. Nuclear Energy* **2019**, *113*, 95.
[31] M. G. Dong, O. Agar, H. O. Tekin, O. Kilicoglu, K. M. Kaky, M. I. Sayyed, *Composites B: Eng.* **2019**, *165*, 636.
[32] Y. S. Alajerami, D. A. Drabold, M. H. A. Mhareb, K. N. Subedi, K. Leslee, A. Cimatu, G. Chen, *J. Appl. Phys.* **2020**, *127*, 175102.
[33] A. Sharma, M. I. Sayyed, O. Agar, H. O. Tekin, *Results Phys.* **2019**, *13*, 102199.
[34] N. Tsoulfanidis, S. Landsberger, *Measurement and Detection of Radiation*, 4th ed., CRC Press, Boca Raton, FL **2015**.
[35] M. G. Sayyed, M. I. Sayyed, M. Çelikbilek Ersundu, A. E. ErsundudPriyank Nayar, M. A. Mahdi, *J. Non-Cryst. Solids* **2017**, *468*, 12.
[36] K. Ashok, M. G. Dong, M. I. Sayyed, G. Lakshminarayana, X. X. Xue, M. A. Mahdi, *Glass Phys. Chem.* **2018**, *44*, 292.
[37] M. I. Sayyed, H. O. Tekin, O. Kilicoglu, O. Agar, M. H. M. Zaid, *Results Phys.* **2018**, *11*, 40.
[38] G. F. Knoll, *Radiation Detection and Measurement.* University of Michigan, Ann Arbor, MI **2002**.
[39] O. S. Shamsan, M. I. Sayyed, D. K. Gaikwad, P. P. Pawar, *Radiat. Phys. Chem.* **2018**, *148*, 86.
[40] M. I. Sayyed, *J. Alloys Compd.* **2017**, *695*, 3191.
[41] F. Akman, R. Durak, M. F. Turhan, M. R. Kacal, *Appl. Radiat. Isot.* **2015**, *101*, 107.
[42] S. Singh, A. Kumar, D. Singh, K. S. Thind, G. S. Mudahar, *Nucl. Instrum. Methods Phys. Res. B* **2008**, *266*, 140.
[43] I. Akkurt, H. Akyildrim, B. Mavi, S. Kilincarslan, C. Basyigit, *Ann. Nucl. Energy* **2010**, *37*, 910.
[44] R. Bagheri, A. Khorrami Moghaddam, H. Yousefnia, *Nucl. Eng. Technol.* **2017** *49*, 216.